

Three-Dimensional Simulation of Realistic Single Electron Transistors

Gianluca Fiori, Marco G. Pala, and Giuseppe Iannaccone, *Member, IEEE*

Abstract—We present an approach, and its implementation in a computer program, for the three-dimensional (3-D) simulation of realistic single electron transistor (SET) structures, in which subregions with different degrees of quantum confinement are simultaneously considered. The proposed approach is based on the self-consistent solution of the many body Schrödinger equation with density functional theory and on the computation of the conductance of tunnel constrictions through the solution of the 3-D Schrödinger equation with open boundary conditions. We have developed an efficient code (ViDES) based on such an approach. As examples of addressable SET structures, we present the simulation of a SET, one defined by metal gates on an AlGaAs/GaAs heterostructures, and of a SET defined by etching and oxidation on the silicon-on-insulator material system. Since SETs represent prototypical nanoscale devices, the code may be a valuable tool for the investigation and optimization of a broad range of nanoelectronic solid-state devices.

Index Terms—Poisson/Schrödinger, silicon-on-insulator (SOI) technology, single electron transistors (SETs), split gates, three-dimensional (3-D) solver.

I. INTRODUCTION

THE improvement of fabrication techniques in the last couple of decades has made possible the realization and characterization of devices capable of exploiting the discreteness of the electron charge. Single electron transistors (SETs) represent the prototype of such types of devices, allowing to control a current consisting of electrons traversing the device one by one, by varying the charge on the control gate by a fraction of an electron [1]. While SETs are extremely and exceedingly sensible to the presence of single charged defects, impressive reproducibility have been recently obtained through refined fabrication techniques [2], [3].

In simulating these types of devices, it is necessary to take into account the effects of quantum confinement, typically three-dimensional (3-D) in the dot region, two-dimensional (2-D) in the wire connecting the dot to reservoirs, and one-dimensional (1-D) in the two-dimensional electron gas (2DEG) reservoirs. This kind of approach has been proposed by Scholze *et al.* [4]: The self-consistent Poisson–Schrödinger equation

Manuscript received August 16, 2004; revised December 1, 2004. This work was supported by the Information Society Technology under NanoTCAD project European Community Contract IST-1999-10828 and by the IST Network of Excellence Silicon Nanodevices.

G. Fiori and G. Iannaccone are with the Dipartimento di Ingegneria dell'Informazione, Università degli Studi di Pisa, 56122 Pisa, Italy.

M. G. Pala was with the Dipartimento di Ingegneria dell'Informazione, Università degli Studi di Pisa, 56122 Pisa, Italy. He is now with the Commission à l'Énergie Atomique–Laboratoire de Electronique de Technologie de l'Information, 38000 Grenoble, France

Digital Object Identifier 10.1109/TNANO.2005.851284

is solved with the density-functional theory, then the device capacitances are extracted from the dependence of the electrochemical potential of the dot on the gate and reservoir voltages, and the constriction conductances are computed in an approximate way, using the 1-D transfer Hamiltonian formalism.

In this paper, we present a code (ViDES) for the self-consistent solution of the many-body Schrödinger equation in a realistic 3-D domain based on density functional theory (DFT) with local density approximation (LDA) [6]. The Poisson equation is solved over the entire 3-D domain, while the solution of the Schrödinger equation is limited to confined regions and solved in the momentum space [7]. The numerical algorithm is based on the Newton–Raphson (NR) method with a predictor corrector scheme simplified with respect to that proposed in [5]. In addition, in order to compute the SET conductance within a 3-D treatment of the transport, we have solved the 3-D Schrödinger equation with open boundary conditions for each quantum constriction by means of the scattering matrix technique. For each constriction, the domain is subdivided in N slices along the propagation direction, and the 2-D Schrödinger equation in the transversal plane is solved for each slice. By enforcing mode matching, we can then compute the total scattering matrix of the constriction and, therefore, the conductance.

This paper is organized as follows. In Section II, we present the physical model used to describe the devices and the adopted numerical methods. In Section III, we show simulation results for a SET defined by split gates on a AlGaAs/GaAs heterostructure, while in Section IV, we show results for a SET fabricated with silicon-on-insulator (SOI) technology [8]. Conclusions follow in Section V.

II. PHYSICAL MODEL AND NUMERICAL METHOD

In order to solve the many-body Schrödinger equation with the mean field approximation in a realistic structure, we have to solve the nonlinear Poisson equation in three dimensions, which reads

$$\nabla[\epsilon(\mathbf{r})\nabla\phi(\mathbf{r})] = -q[p(\mathbf{r}) - n(\mathbf{r}) + N_D^+(\mathbf{r}) - N_A^-(\mathbf{r}) + \rho_{\text{fix}}] \quad (1)$$

where ϕ is the electrostatic potential, ϵ is the dielectric constant, p and n are the hole and electron densities, respectively, N_D^+ is the concentration of ionized donors, N_A^- is the concentration of ionized acceptors, and ρ_{fix} is the fixed charge density.

While a semiclassical approximation is assumed in the whole domain for hole, acceptor, and donor densities, the electron density in strongly confined regions is computed by solving the Schrödinger equation with the DFT and LDA [9]–[11]. Elsewhere, also for the electron density, the semiclassical expression

is used. The Schrödinger equation for the Kohn–Sham single electron states reads

$$-\frac{\hbar^2}{2}\nabla[m^{-1}(\mathbf{r})\nabla\Psi(\mathbf{r})] + V(\mathbf{r})\Psi(\mathbf{r}) = E\Psi(\mathbf{r}) \quad (2)$$

where \hbar is the reduced Planck's constant, m is the effective mass tensor, and Ψ and E are the eigenfunctions and eigenvalues, respectively. The confining potential V can be expressed as $V = E_c + V_{\text{exc}}$, where E_c is the conduction band edge and V_{exc} is the exchange-correlation potential [6]

$$V_{\text{exc}} = -\frac{q^2}{4\pi^2\epsilon_0\epsilon_r} [3\pi^2 n(\mathbf{r})]^{\frac{1}{3}}. \quad (3)$$

Here, we use the expression valid for a 3-D system, which we have found to have an impact on the results only inside the dots. It turns out that exchange-correlation corrections to the potential are negligible in other regions of the analyzed structures. Even if the region is not strictly closed, in the sense that tunneling out has a nonzero probability, we assume null Dirichlet boundary conditions for the eigenfunctions. As long as tunnel barriers are opaque (tunneling probability much smaller than one) and the boundaries of the confined region are taken in order to allow penetration of the wave function in the barriers, such approximation has a negligible effect on the energy eigenvalues and on the shape of the eigenfunctions.

The coupled Poisson and Schrödinger equations are solved by means of an NR method with a predictor–corrector scheme, which we have verified to be faster and more stable than a code previously developed by our group, based on the multigrid algorithm [16]. The Schrödinger equation is solved at the beginning of each NR cycle. The eigenfunctions are then kept constant until the NR cycle converges, while the eigenvalues are adjusted according to the mentioned predictor–corrector scheme [5]. At the end of the NR cycle, the Schrödinger equation is solved again and a new NR cycle is performed. The algorithm is ended when the norm-two of the difference between the electrostatic potentials obtained at the end of two successive NR cycles is smaller than a given threshold. We sketched a flowchart of the whole code in Fig. 1: an initial potential Φ_i is used to compute the local density of states by solving the Schrödinger equation; the local density of states is then frozen and the nonlinear Poisson equation is solved with an NR algorithm in order to obtain the potential Φ_f . If Φ_f is not close enough to Φ_i , a new cycle is started by again computing the local density of states. In this case, we also verified that the residual term of the Poisson equation was approximately one-millionth of the electronic charge.

From a numerical point-of-view, the main problem is represented by the memory and the computational resources required for the solution of the 3-D Schrödinger equation. Our approach allows us to keep such requirements under control by solving the Schrödinger equation in the momentum space with a method developed and discussed in [7]. The main advantage in solving the Schrödinger equation in the momentum space consists of the possibility to use a smaller number of basis elements to properly describe the solutions corresponding to the smaller energies, which correspond to occupied states. A sine fast Fourier

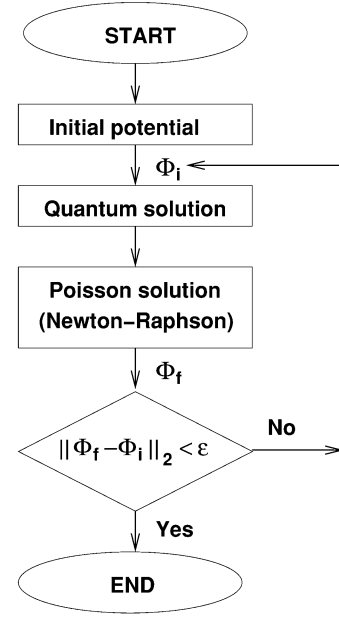


Fig. 1. Flowchart of the self-consistent 3-D Poisson–Schrödinger solver.

transform is used to transfer in the momentum space the physical quantities defining the problem, but not to directly solve (2). Indeed, once the eigenvalue problem is transferred into the momentum space through the sine fast Fourier transform, we can solve the eigenvalue problem on a reduced matrix and then antitransform the eigenfunctions in the real space. If confinement is quite strong, as is often the case, we can have a substantial reduction of the matrix size in the momentum space, typically by a factor of two in each direction, which means a factor of eight in the matrix size. After such a reduction, we can even use standard full diagonalization algorithms since the time for the solution of the eigenvalue problem becomes a small fraction of the overall computing time, and there is a small marginal advantage in making use of more sophisticated algorithms.

Concerning the 3-D quantum region, the quantum dot, the number of electrons in the confined region is fixed to N , and the electron density can be expressed as

$$n(\mathbf{r}) = 2 \sum_{i=1}^m |\psi_i(\mathbf{r})|^2 + (N - 2m) |\psi_{m+1}(\mathbf{r})|^2 \quad (4)$$

where ψ_i is the orbital associated to the i th eigenvalue, and $m = [(N/2)]$ is the number of fully occupied single electron levels.

For a given N , the electrochemical potential of the dot can be determined in a simple way by means of the Slater formula [12]. Indeed, the electrochemical potential $\mu(N)$, defined as the energy necessary to add the N th electron to the dot, can be expressed as

$$\mu(N) = E(N) - E(N - 1) = \varepsilon \left(N - \frac{1}{2} \right) \quad (5)$$

where E is the total energy of the dot, while ε is the energy of the half-occupied highest Kohn–Sham orbital of a system with $N - (1/2)$ electrons.

Once we obtain the band and density profiles at quasi-equilibrium, we can compute the transport properties of the device. In

order to compute the conductance between two generic subregions (nodes) of the device, we solve the 3-D Schrödinger equation with open boundary conditions along the direction of propagation.

We obtain the quantum conductance G at zero temperature using the Landauer–Büttiker formula [13], [14] that expresses G as a function of the transmission matrix t

$$G(E) = \frac{2q^2}{h} \text{Tr} \left\{ t^\dagger t \right\} \quad (6)$$

where q is the electron charge and h is Planck's constant. The numerical method is based on the computation of the scattering matrix of the conductor. First, the domain is subdivided in several slices along the propagation direction. For each slice j , one can easily compute the scattering matrix S_j by solving the 2-D Schrödinger equation with Dirichlet boundary conditions on the transversal cross section. S_j has the form

$$S_j = \begin{pmatrix} r_j & t'_j \\ t_j & r'_j \end{pmatrix} \quad (7)$$

where $t_j(t'_j)$ and $r_j(r'_j)$ are the transmission and reflection matrices, respectively, from the left- to right-hand side (right- to left-hand side). Note also that S_j satisfies the relation $S_j S_j^\dagger = I$ that implies current continuity. In order to compute the total scattering matrix S_T , it is sufficient to compose all the S_j matrices by enforcing continuity of the wave function and of the probability current density [15].

At low temperatures, current through the central dot—in the limit of the linear transport regime—is allowed only when the electrochemical potential of the dot aligns with the Fermi energy of the two reservoirs and is characterized by a series of peaks, whose broadening depends on the temperature. The height of such peaks depends on the geometry of the dot and of the tunneling barriers and is proportional to the transmission probability of one electron through the barrier. The transmission probability T is related to the tunneling rate Γ via the generic relation $\Gamma = T \cdot \nu$, where ν is the attempt frequency. We are interested in the energy regime $K_B T \ll \Delta \ll q^2/C$, where the generic conductance formula, given in [22], holds as follows:

$$G = G_{\max} \cosh^{-2} \left(\frac{\Delta(N_{\min})}{2K_B T} \right) \quad (8)$$

$$G_{\max} = \frac{q^2}{4K_B T} \frac{\Gamma^l \Gamma^r}{\Gamma^l + \Gamma^r}. \quad (9)$$

Here, Γ^l and Γ^r are the tunneling rates corresponding to the left- and right-hand-side leads, respectively, whereas N_{\min} is the number of electrons in the dot that minimizes the absolute value of $\Delta(N) = E_N + U(N) - U(N-1) - E_F$, which represents the level that almost totally contributes to conduction, $U(N)$ is the electrostatic energy of the dot, and E_N is the energy level. Comparing the notation of [22] with ours, we note that $\Delta(N_{\min})$ corresponds to $\mu(N_{\min}) - E_F$ for the values of V_G for which $\mu(N_{\min}) \sim E_F$.

The values of Γ^l and Γ^r are computed using the mentioned method for the computation of the scattering matrix of the 3-D

potential that defines the constriction. For such computation, that voltage applied to the control gate is the value for which the electro-chemical potential in the dot aligns with the Fermi energy of the leads, i.e., in correspondence with each peak of the Coulomb oscillations of the conductance as a function of the control gate voltage.

III. SET ELECTROSTATICALLY DEFINED BY METAL GATES ON AN AlGaAs/GaAs HETEROSTRUCTURE

Here, we consider a SET defined by split gates on an AlGaAs/GaAs modulation doped heterostructure. We consider such a device as a typical testbench structure due to the popularity of structures defined by gate voltages. Further, at the same time, it presents two kinds of different quantum confinement since we have 3-D confinement inside the dot and 1-D confinement along the 2-D electron gas at the interface. Physically, such a SET is interesting since it is characterized by a variable size of the dot depending on the number of electrons in the central island and by shell-filling effects.

The layer structure is shown in Fig. 2(a) and consists of a p-doped GaAs bulk layer with unintentional acceptor concentration of 10^{15} cm^{-3} on which a 20-nm intrinsic AlGaAs spacer is grown, then a 50-nm AlGaAs n-doped layer with donor concentration of approximately 10^{18} cm^{-3} , and a 10-nm GaAs cap layer.

In Fig. 2(b), the gate layout considered in the simulation is shown.

Surface states have been considered on the exposed surface at the top of the structure. Indeed, the region in which electron transport occurs is very close to the surface so device characteristics are strongly affected by surface properties. We have assumed a model for surface states typically applied to metal–semiconductor interfaces [17] and based on two parameters: an effective work function Φ^* and a uniform density of surface states per unit area per unit energy D_s [18]. We assume that all the surface states below the effective work function behave as donors and all the states above as acceptors. Here, we use parameters for the surface state model extracted from measurements on similar structures [19]: $\Phi^* = 4.85 \text{ eV}$ and $D_s = 5 \times 10^{12} \text{ cm}^{-2} \text{ eV}^{-1}$. Donor concentration has been taken as $N_D = 3.5 \times 10^{17} \text{ cm}^{-3}$.

In the 2DEG, two kinds of confinement have been considered. As shown in Fig. 2(b), in the center of the 2DEG, the 3-D Schrödinger equation has been solved since quantum confinement is strong in all three directions while, in the rest of the 2DEG, the Schrödinger equation has been solved only in the vertical direction since confinement along the direction perpendicular to the AlGaAs/GaAs interface is predominant. Regarding the corrections due to exchange–correlation effects, we have found that they are significant only in the 3-D confinement region, whereas in the 1-D confinement region, using the expression for the exchange–correlation potential in a 2-D system given in [20], they are smaller by more than one order of magnitude and, hence, can be neglected with respect to the energy level spacing in a 2DEG. The boundaries of the 3-D regions are chosen in such a way that Dirichlet boundary conditions on the

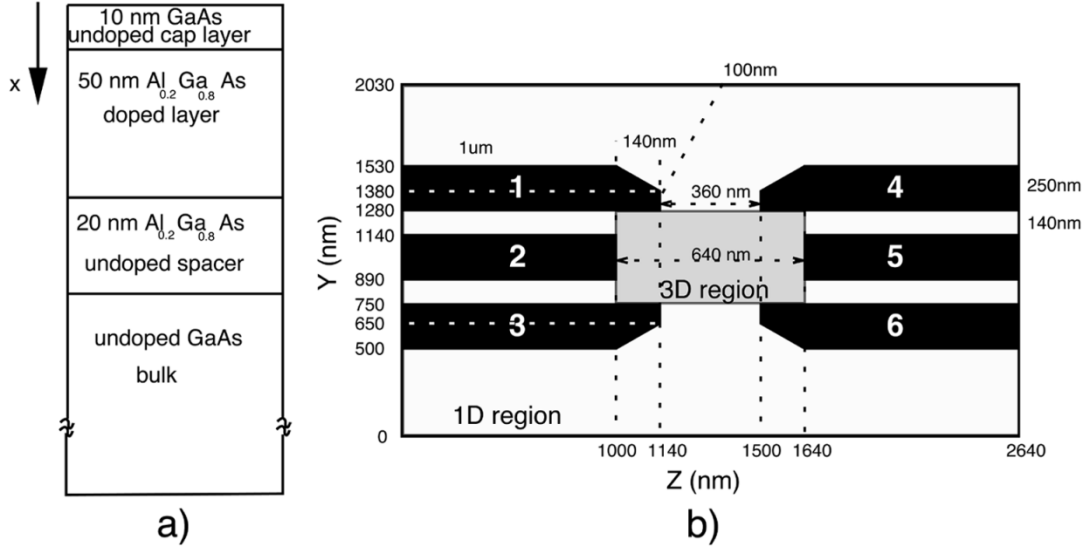


Fig. 2. (a) Layer structure and (b) gate layout of the SET defined by split gate on an AlGaAs/GaAs heterostructure. In this figure, the regions are shown in which 1-D and 3-D quantum electron density has been computed. Gates 1, 3, 4, and 6 are the external gates that define the quantum dot, while 2 and 3 are the inner gate pair that determine the number of electrons in the dot.

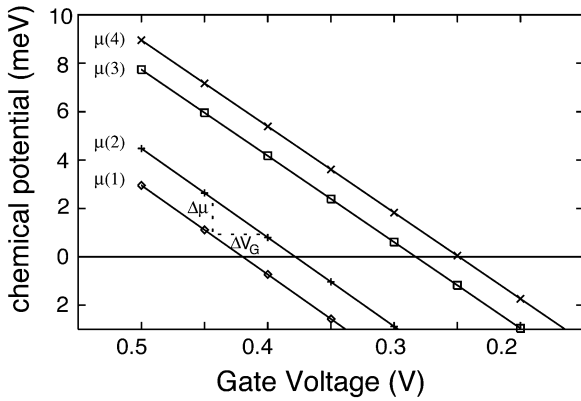


Fig. 3. Electrochemical potential as a function of the inner gate voltage for a number of electrons ranging from 1 to 4.

wave function can be imposed without introducing artifacts in the electron density.

Fig. 3 shows the computed electrochemical potential as a function of the inner gate pair voltage (V_G) for a fixed external gate voltage ($V_{G1} = -1.1$ V). From these curves, it is possible to extract the capacitance C_g between the dot and inner gates (gates 2 and 5) and the total capacitance C_T defined as

$$C_T = 2C_j + C_g + C_m \quad (10)$$

where C_j is the capacitance between the dot and each reservoir and C_m is the capacitance between the dot and the other gates (gates 1, 3, 4, 6). Fig. 4 shows the equivalent circuit of the SET. In particular [21], we have

$$C_T = \frac{q}{\Delta\mu} \Big|_{V_G}; \quad C_g = \frac{q}{\Delta V_G} \Big|_{\mu} \quad (11)$$

where ΔV_G and $\Delta\mu$ are the distances between two curves that differ by one electron at constant μ and V_G , respectively, as shown in Fig. 3.

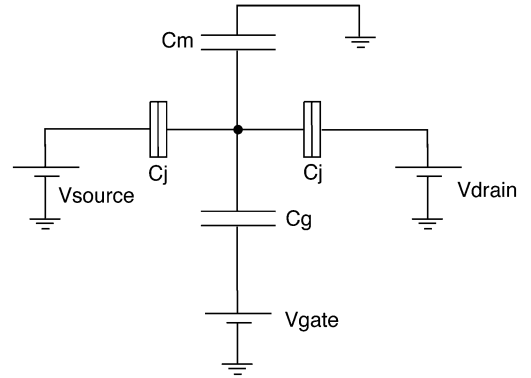


Fig. 4. Equivalent circuit of the AlGaAs/GaAs SET device.

TABLE I
TOTAL DOT CAPACITANCE AND GATE-DOT CAPACITANCE DERIVED FROM SIMULATIONS AS A FUNCTION OF THE NUMBER OF ELECTRONS IN THE DOT FOR THE AlGaAs/GaAs SET

transition (# electrons)	1 → 2	2 → 3	3 → 4
C_g	3.84 aF	1.68 aF	4.67 aF
C_T	105.21 aF	46.93 aF	131.95 aF
C_j	0.713 aF	0.297 aF	0.805 aF
C_m	99.94 aF	44.66 aF	125.67 aF

TABLE II
GATE VOLTAGES CORRESPONDING TO CONDUCTANCE PEAKS OF THE AlGaAs/GaAs SET

Peak number	1	2	3	4
Voltage (V)	-0.420	-0.379	-0.283	-0.249

Curves are almost linear and parallel, but are not equally spaced. This means that while C_T and C_g vary as the number of electrons in the dot increase, the ratio C_T/C_g remains constant.

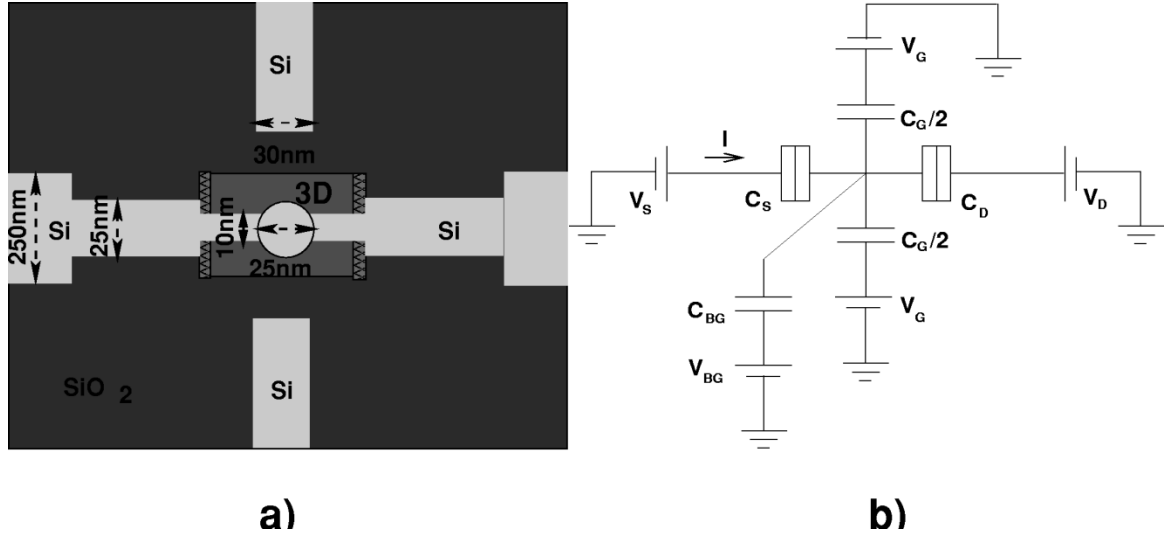


Fig. 5. (a) Schematic view of the central region of the simulated SOI SET extracted from an SEM image in [8]. (b) Equivalent circuit for the SOI SET.

The values of the capacitance extracted from Fig. 3 are written in Table I. C_j is similarly obtained as

$$C_j = \frac{q}{\Delta V_D} \Big|_{V_G} \quad (12)$$

where ΔV_D is defined as $V_{D0}(N) - V_{D0}(N-1)$, where $V_{D0}(N)$ is the drain voltage required to have $\mu(N) = 0$ eV for a given V_G . The remaining C_m capacitance can be obtained from (10). C_j are quite small for the considered structure, meaning that the dot is weakly coupled to the reservoirs.

From Fig. 3, we can also extract the gate voltages for which the dot electrochemical potential is equal to the Fermi level of the reservoirs, at which conductance exhibits a peak (Table II). In this case, an odd–even pairing is evident in the position of the conductance peaks, and is due to the fact that each Kohn–Sham orbital is occupied by two electrons, and the conduction band in GaAs has a single minimum at the Γ point.

In the case of the GaAs SET, we do not show simulation results on conductance since, for a small number of electrons in the dot, the dot is so small and weakly coupled to the reservoirs that conductance is negligibly small. In reality, that would correspond to a dot that becomes practically insulated from the reservoirs even when it still contains several electrons.

IV. SOI SET

We now focus on the SOI SET fabricated and characterized at the University of Tübingen, Tübingen, Germany, by Augke *et al.* [8]. The structure is fabricated on an n-doped layer of silicon with donor concentration $N_D = 3 \times 10^{18} \text{ cm}^{-3}$ fabricated on an SOI wafer. In Fig. 5(a), the sketch of the simulated structure extracted from an SEM image in [8] is shown. The SET consists of two silicon side gates and of a silicon dot in the center separated from source and drain by tunnel barriers. The silicon layer is separated from the back gate by an oxide of 400 nm.

In Fig. 5(b), the equivalent circuit of the SET is shown, consisting of two tunneling capacitances C_S and C_D between the source and drain reservoirs and dot, respectively, two side gate

capacitances $C_G/2$, and the dot-to-backgate capacitance C_{BG} . The total capacitance C_T can be expressed as $C_T = C_G + C_D + C_S + C_{BG}$.

As explained in Section III, in order to estimate the device capacitances shown in Fig. 5(b), we are primarily interested in evaluating the electrochemical potential of the dot. In solving the 3-D Poisson–Schrödinger equation for the computation of the confinement potential, we have assumed that the central dot region is a 3-D quantum confinement area even if it is connected to the leads via tunneling junctions. This approximation holds very well since typical conductance values through such junctions are much smaller than the quantum conductance unity e^2/h , as further verified. In addition, since the silicon conduction band has six minima in the momentum space, the eigenvalue problem has to be solved three times, one of each axis of the momentum space. Kohn–Sham orbitals of the six minima are then grouped together and ordered in terms of increasing eigenvalue. Therefore, each Kohn–Sham orbital has a degeneracy of four (two for spin and two for the couple of minima on each momentum axis). In addition, if the 3-D quantum region does not present regions of preferential confinement, the first 12 electrons occupy quasi-degenerate Kohn–Sham orbitals.

In Fig. 6, we show the electrochemical potential as a function of gate voltage for various N . The corresponding capacitance values computed via (11) are shown in Table III. We want to emphasize that the capacitance values are very sensitive to the geometry of the structure. This indicates the fundamental role played by the extraction of a correct geometry from experimental data. In fact, it can be readily seen that different 3-D geometries may be extracted that are consistent with the scanning electron microscopy (SEM) micrograph in [8]. To evaluate such an aspect, we have performed simulations on two different geometries [as shown in Table III(a) and (b)], both compatible with the SEM image. In particular, in Table III, we show the capacitance values obtained for the two structures and the experimental measurements given in [8]. Even if the results for the structures shown in Table III(a) and (b) have the same order of magnitude of the experimental data, it is clear that the results are

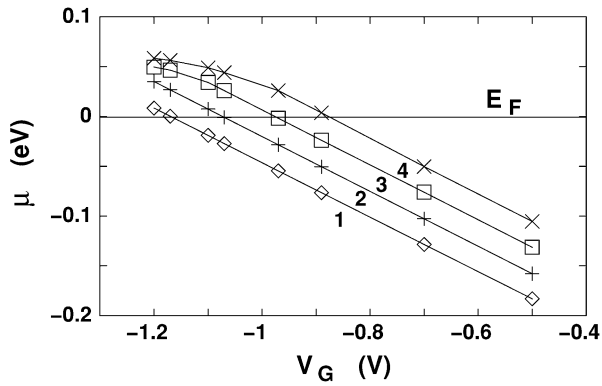


Fig. 6. Electrochemical potential of the dot for a varying number of electrons as a function of V_G for the prismatic structure. Peaks correspond respectively to $N = 1, 2, 3, 4$ and temperature is 4.2 K.

TABLE III
COMPARISON BETWEEN SIMULATION CAPACITANCE AND
EXPERIMENTAL DATA FOR THE SOI SET [8]

capacitance	(a) structure	(b) structure	experiments
C_T	6 aF	22 aF	32 aF
C_G	1.6 aF	4 aF	3.4 aF
C_D	1 aF	6 aF	16 aF

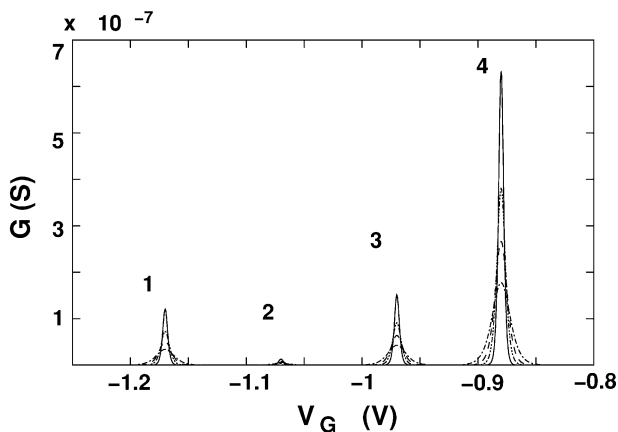


Fig. 7. Coulomb blockade oscillations obtained as V_G is varied for the prismatic structure. Temperature is 4.2, 7, 10, and 15 K. The oscillation period is 0.1 V.

very sensitive to the dot shape. Indeed, SETs are structures very sensitive to minimal variations of the sample and exhibit quite different behaviors from sample to sample. It turns out that the change of some nanometers in the dot size or the presence of surface defects can significantly modify the expected characteristics.

Finally, in Fig. 7, we plot the conductance oscillations corresponding to the intersection points in Fig. 6. Comparing our results with the corresponding experimental curves in [8], we verify that the conductances differ by a factor of ten, i.e., peaks are approximately 10^{-7} S for simulations and approximately 10^{-8} S for experimental data, while the oscillation period is approximately 100 mV for simulations and approximately 50 mV

for experimental data. Discrepancies in the transport properties are mainly due to the lack of information on the size and shape of the dot. As shown in Table III, the choice of a different geometry of the same dot to obtain gate capacitances differing by a factor of two is sufficient. Given only the partial knowledge of the structure geometry and the sensitivity of tunneling conductance on the geometrical details, we believe that the agreement with the experiment is satisfactory.

V. CONCLUSION

In this paper, we have presented a 3-D simulation approach for nanoscale devices in which subregions with different types of confinement are present, focusing in particular on SETs defined by split gates on AlGaAs/GaAs heterostructures and on SOI substrates. Indeed, SETs are a very useful testbench for assessing the capabilities of codes for the simulation of nanoelectronic solid-states devices.

We have shown that the method allows to take into account the detailed geometry of the structure, and that the code allows to compute parameters useful for a higher level description of device behavior, in terms of normal and tunneling capacitances, to be exploited by circuit simulators,

The 3-D self-consistent Poisson–Schrödinger equation has been solved using efficient algorithms based on the NR algorithm and on a Schrödinger solver operating in a reduced momentum space [7]. The conductance of 3-D tunneling constrictions has been computed by solving the 3-D Schrödinger equation with open boundary conditions with a scattering matrix technique.

The code we have presented runs on a low-end workstation, and may represent a valuable tool for the investigation and optimization of nanoelectronic devices based on building blocks in which carriers are strongly confined.

REFERENCES

- [1] K. Likharev, "Single-electron devices and their applications," *Proc. IEEE*, vol. 87, no. 4, pp. 606–632, Apr. 1999.
- [2] A. Fujiwara, Y. Takahashi, K. Yamazaki, H. Namatsu, M. Nagase, K. Kurihara, and K. Murase, "Double-island single-electron devices: A useful unit device for single-electron logic LSI's," *IEEE Trans. Electron Devices*, vol. 46, no. 5, pp. 954–959, May 1999.
- [3] K. Nishiguchi, H. Inokawa, Y. Ono, A. Fujiwara, and Y. Takahashi, "Automatic control of oscillation phase of a single-electron transistor," *IEEE Electron Device Lett.*, vol. 25, no. 1, pp. 31–33, Jan. 2004.
- [4] A. Scholze, A. Schenk, and W. Fichtner, "Single-electron device simulation," *IEEE Trans. Electron Devices*, vol. 47, no. 10, pp. 1811–1818, Oct. 2000.
- [5] A. Trellakis, A. T. Galick, A. Pacelli, and U. Ravaioli, "Iteration scheme for the solution of the two-dimensional Schrödinger–Poisson equations in quantum structures," *J. Appl. Phys.*, vol. 81, pp. 7800–7804, 1997.
- [6] J. C. Inkson, *Many Body Theory of Solids—An Introduction*. New York: Plenum, 1984.
- [7] M. G. Pala and G. Iannaccone, "A three-dimensional solver of the Schrödinger equation in momentum space for the detailed simulation of nanostructures," *Nanotechnology*, vol. 13, pp. 369–372, 2002.
- [8] R. Augke, W. Eberhardt, C. Single, F. E. Prins, D. A. Wharam, and D. P. Kern, "Doped silicon single electron transistors with single island characteristics," *Appl. Phys. Lett.*, vol. 76, pp. 2065–2067, 2000.
- [9] H. Hohenber and W. Kohn, "Inhomogeneous electron gas," *Phys. Rev.*, vol. 136, pp. B864–B871, 1964.
- [10] W. Kohn and L. J. Sham, "Self-consistent equations including exchange and correlation effects," *Phys. Rev. A*, vol. 140, pp. A1133–A1138, 1965.
- [11] U. von Barth and L. Hedin, "A local exchange-correlation potential for the spin polarized case," *J. Phys. C*, vol. 5, pp. 1629–1642, 1972.

- [12] J. C. Slater, "A simplification of the Hartree–Fock method," *Phys. Rev.*, vol. 81, pp. 385–390, 1951.
- [13] R. Landauer, "Spatial variation of currents and fields due to localized scatterers in metallic conduction," *IBM J. Res. Dev.*, vol. 1, pp. 223–231, 1957.
- [14] M. Büttiker, "Symmetry of electrical conduction," *IBM J. Res. Dev.*, vol. 32, pp. 317–334, 1988.
- [15] S. Datta, *Electronic Transport in Mesoscopic Systems*. Cambridge, U.K.: Cambridge Univ. Press, 1995.
- [16] W. H. Press, S. A. Teukolsky, W. T. Vetterling, and B. P. Flannery, *Numerical Recipes in Fortran*, 2nd ed. New York: Cambridge Univ. Press, 1992, vol. 77.
- [17] S. Sze, *Physics of Semiconductor Devices*, 2nd ed. New York: Wiley, 1981, pp. 270–279.
- [18] G. Fiori and G. Iannaccone, "The effect of quantum confinement and discrete dopants in nanoscale 50 nm n-MOSFETs: A three-dimensional simulation," *Nanotechnology*, vol. 13, p. 294, 2002.
- [19] M. G. Pala, G. Iannaccone, S. Kaiser, A. Schliemann, L. Worschech, and A. Forchel, "Extraction of parameters of surface states from experimental test structures," *Nanotechnology*, vol. 13, pp. 373–377, 2002.
- [20] F. Stern, "Electron exchange energy in Si inversion layers," *Phys. Rev. Lett.*, vol. 30, pp. 278–280, 1973.
- [21] M. Macucci, K. Hess, and G. J. Iafrate, "Electronic energy spectrum and the concept of capacitance in quantum dots," *Phys. Rev. B*, vol. 48, pp. 17 354–17 363, 1993.
- [22] C. W. J. Beenakker, "Theory of Coulomb-blockade oscillations in the conductance of a quantum dot," *Phys. Rev. B*, vol. 44, pp. 1646–1656, 1991.



Gianluca Fiori received the Electronic Engineering degree and Ph.D. degree in electronic engineering from the Università di Pisa, Pisa, Italy, in 2001 and 2005, respectively. His doctoral thesis concerned approaches for the simulation of 3-D nanoelectronic devices.

His main field of activity is the development of models and codes for the simulations of semiconductor nanoscale devices.



Marco G. Pala received the Physics degree and Ph.D. degree in electrical engineering from the Università di Pisa, Pisa, Italy, in 2000 and 2004, respectively.

From October 2002 to July 2003, he was with the University of Karlsruhe, Karlsruhe, Germany, where he was mainly involved with spin-dependent problems in nanostructures. His main interests concern analytical and numerical studies of transport properties of carriers in mesoscopic structures. He is currently with the Commission à l'Énergie Atomique (CEA)–Laboratoire de Electronique de Technologie de l'Information (LETI), Grenoble, France, where he is involved with the simulation of innovative MOSFET devices.



Giuseppe Iannaccone (M'98) was born on April 28, 1968. He received the Laurea degree (*cum laude*) in electrical engineering and Ph.D. degree from the Università di Pisa, Pisa, Italy, in 1992 and 1996, respectively. His doctoral thesis concerned transport and noise phenomena in ultrasmall structures.

Since January 2001, he has been an Associate Professor with the Dipartimento di Ingegneria dell'Informazione, Università degli Studi di Pisa. He has authored over 90 papers in peer-reviewed journals and 60 papers in proceedings of international conferences. His interests include transport and noise modeling in nanoscale devices, devices and architectures for nanoelectronics, the design of passive RF identification (RFID) transponders, and the exploitation of quantum effects in conventional electron devices. He has participated in a series of European and National research projects as consortium coordinator or principal investigator.